J Nanopart Res (2014) 16:2664
DOI 10.1007/s11051-014-2664-z

RESEARCH PAPER

Silica nanoparticles mediated neuronal cell death in corpus striatum of rat brain: implication of mitochondrial, endoplasmic reticulum and oxidative stress

Arshiya Parveen · Syed Husain Mustafa Rizvi · Farzana Mahdi · Sandeep Tripathi · Iqbal Ahmad · Rajendra K. Shukla · Vinay K. Khanna · Ranjana Singh · Devendra K. Patel · Abbas Ali Mahdi

Received: 6 April 2014 / Accepted: 20 September 2014 / Published online: 22 October 2014

Abstract Extensive uses of silica nanoparticles (SiNPs) in biomedical and industrial fields have increased the risk of exposure, resulting concerns about their safety. We focussed on some of the safety aspects by studying neurobehavioural impairment, oxidative stress (OS), neurochemical and ultrastructural changes in corpus striatum (CS) of male Wistar rats exposed to 80-nm SiNPs. Moreover, its role in inducing mitochondrial and endoplasmic reticulum (ER) stress-mediated neuronal apoptosis was also investigated. The results demonstrated impairment in neurobehavioural indices, and a significant increase in lipid peroxide levels (LPO), hydrogen peroxide (H_2O_2), superoxide (O_2^-) and protein carbonyl content, whereas there was a significant decrease in the activities of the enzymes, manganese superoxide dismutase (Mn SOD), glutathione peroxidase (GPx), catalase (CAT) and reduced glutathione (GSH) content, suggesting impaired antioxidant defence system. Protein (cytochrome *c*, Bcl-2, Bax, p53, caspase-3, caspase 12 and CHOP/Gadd153) and mRNA (Bcl-2, Bax, p53 and CHOP/Gadd153, cytochrome *c*) expression studies of mitochondrial and ER stress-related apoptotic factors suggested that both the cell organelles were involved in OS-mediated apoptosis in treated rat brain CS. Moreover, electron microscopic studies clearly showed mitochondrial and ER dysfunction. In conclusion, the result of the study suggested that subchronic SiNPs' exposure has the potential to alter the behavioural activity and also to bring about changes in biochemical, neurochemical and ultrastructural profiles in CS region of rat brain. Furthermore, we also report SiNPs-induced apoptosis in CS, through mitochondrial and ER stress-mediated signalling.

We dedicate this paper in memory of late Padam Shri Prof. Mahdi Hasan, a renowned neuroscientist who was motivator for this study but unfortunately died on 12th January 2013.

A. Parveen · S. H. M. Rizvi · R. Singh · A. A. Mahdi (✉)
Department of Biochemistry, King George's Medical University, Lucknow 226003, Uttar Pradesh, India
e-mail: abbasalimahdi@gmail.com

F. Mahdi
Department of Biochemistry, Era's Lucknow Medical College & Hospital, Lucknow, India

S. Tripathi
Department of Biotechnology, Institute of Engineering and Technology, Jaipur, India

I. Ahmad
Fibre Toxicology, CSIR-Indian Institute of Toxicology Research, Lucknow, India

R. K. Shukla · V. K. Khanna
Developmental Toxicology, CSIR-Indian Institute of Toxicology Research, Lucknow, India

D. K. Patel
Analytical Chemistry Division, CSIR-Indian Institute of Toxicology Research, Lucknow, India

Keywords Silica nanoparticles · Corpus striatum · Neuronal apoptosis · Mitochondrial stress · Endoplasmic reticulum stress · Oxidative stress

Introduction

In recent years, numerous toxicological investigations of engineered nanoparticles have been carried out (Liao et al. 2009; Brouwer 2010), and there are several reports that inhaled or injected nanoparticles can cross the blood–brain barrier (Lockman et al. 2004) and enter the central nervous system (CNS) of the exposed animals (Elder et al. 2006). Inhaled nanoparticles either translocate directly into the brain or exit the lungs and enter the circulation (Oszlanczi et al. 2011). Ultrafine carbon black (ufCB), nano- and submicron ferric oxide (Fe_2O_3), titanium dioxide (TiO_2), manganese oxide (MnO_2) and silver nanoparticles have been found to translocate into the brain via the olfactory nerve pathway after intranasal instillation exposure. Moreover, there are reports that these nanoparticles also accumulate in different brain regions and stimulate OS, inflammatory responses, pathological changes and impair neural function in the hippocampus and CS (Win Shwe et al. 2006; Wang et al. 2008, 2009a, b; Elder et al. 2006; Takenaka et al. 2001). In view of the above reports, it is necessary to assess the potential of these nanoparticles to contribute to neurotoxicity.

SiNPs have attracted extensive interest due to their easy surface modifications and highly hydrophilic properties, and potential applications in biomedical and industrial fields. These applications include industrial manufacturing, packaging, mechanical polishing, additive to food, cosmetics, optical imaging, targeted drug delivery, cancer therapy and control drug release for gene and protein (Bharali et al. 2005; Slowing et al. 2007; Bottini et al. 2007). The emerging commercialization of SiNPs products have also raised concerns about their safety. There have been reports that SiNPs may pose a health threat by adversely affecting cell function through production of reactive oxygen species (ROS). Experimental evidences, both in vivo and in vitro, support that SiNPs induce intracellular OS and trigger mitochondrial stress-mediated apoptosis (Wu et al. 2011a, b; Liu and Sun 2010; Parveen et al. 2012). Although mitochondria may play a central role in stress-induced neuronal apoptosis by the activation of p53 (Kroemer et al. 2007), mitochondria are not the only cellular organelles that respond to OS-mediated damages. Studies suggest that even ER is also quite sensitive to OS-mediated damage (Chen et al. 2008; Sanges and Marigo 2006; Walter and Hajnoczky 2005). There is growing evidence that ER may also regulate neuronal apoptosis in stressful conditions (Galehdar et al. 2010). It is well known that perturbations of ER homeostasis affect protein folding and cause ER stress in many neurological disorders including Parkinsonism and Alzheimer's disease (Doyle et al. 2011). ER stress can also result in apoptosis through activation of CHOP and caspase-12 pathways (Rizvi et al. 2014; Galehdar et al. 2010; Nakagawa et al. 2000). However, ER stress-mediated apoptosis has received very scanty attention, especially in the field of nanoparticle research. Only a few in vitro studies on nanoparticles showed that ER may play an important role in response to apoptosis and OS-induced damages (Zhang et al. 2012; Christen et al. 2013). However, we hypothesize that, in vivo, ER may play an important role, along with mitochondria, in SiNPs-induced neurotoxicity and neuronal cell death.

To the best of our knowledge, this is the first in vivo study to illustrate that SiNPs may induce ER stress or potentiate ER stress responses along with mitochondrial stress signalling. In the present study, we report behavioural, biochemical, neurochemical and ultrastructural changes in CS region of rat brain exposed to SiNPs. In this study, we also demonstrate SiNPs-induced apoptosis in CS through mitochondrial and ER stress-mediated signalling.

Materials and methods

Silica nanoparticles and characterization

Silica (SiO_2) nanopowder (Product No. 4830HT, average particle size: 80 nm, specific surface area: 440 m^2/g, purity: 99.0 % trace metals basis) was purchased from Nanostructured & Amorphous Materials, Inc. (Houston, TX, USA). The detailed characteristics provided by the supplier are given in Table 1A. The size and shape of the particles were characterized by scanning and transmission electron microscopy (SEM, JEOL JEM-200CX, TEM, FEI

Table 1 (A) Data provided by supplier. (B) Dynamic light scattering (DLS) measurement of SiNPs

A						
Data provided by manufacturer. Note The purity of nanoparticles						
Nanoparticle products IDs	Nanoparticle size	Chemical formulae	Purity (%)	SSA[b] (m^2/g)	Colour	Morphology
4830 HT	80 nm (APS)[a]	SiO_2, amorphous	99.0	440	White	Spherical
B						
DLS measurement of silica nanoparticles						
Parameter					In phosphate buffer saline	
Hydro dynamic size (nm)					397 ± 0.7	
Zeta potential (−mV)					25 ± 0.6	

Data provided by manufacturer. *Note* The purity of nanoparticles

[a] *APS* average particle size

[a] Specific surface area measured by (BET) (Brunauer–Emmett–Edward)

Tecnai G2 Spirit Twin, Czech Republic). Hydrodynamic size and zeta potential of SiNPs in phosphate buffer saline (PBS) were determined by dynamic light scattering (DLS) on a Malvern Instrument (Nano ZS90; Malvern Instruments, Westborough, MA, USA). Briefly, dry powder of SiNPs was suspended in PBS solution, the suspension was sonicated at room temperature for 15 min at 40 W, and the measurements were performed.

Animal and experimental design

Young male rats of Wistar strain ($N = 60$) weighing around 150–200 g, obtained from the central animal house of CSIR-Indian Institute of Toxicology Research (CSIR-IITR), Lucknow were used in the study. Rats were housed in an air conditioned room at a temperature of 25 ± 2 °C with a 12-h light/dark cycle under standard hygiene conditions. They had free access to pellet diet (procured from national supplier) and water ad libitum. The study was approved by the Institutional Animal Ethics Committee (IAEC) of King George's Medical University, Lucknow, India, and all experiments were carried out in accordance with the guidelines laid down by the Committee for the Purpose of Control and Supervision of Experiments on Animals (CPCSEA), Ministry of Environment and Forests (Government of India), New Delhi, India.

The animals were randomly divided into five groups, each group comprising 12 rats (6 controls and 6 treated rats each). Rats in Group I were treated with 80-nm SiNPs (150 μg/50 μl PBS/rat), intranasally instilled into both nostrils, using micro-syringe, for 15 days. Rats in Group II, III, IV and V were also treated with 80-nm SiNPs (150 μg in 50 μl PBS/rat) similarly as Group I, for 90 days. Before intranasal instillation, SiNPs were suspended into PSB and sonicated for 15–20 min and mechanically vibrated for 2 or 3 min to prevent aggregation and to keep the maximum dispersed state of particles in PBS. Control rats were treated with PBS (50 μl/rat) for the duration of the treatment. At post instillation day 15, rats in Group I were sacrificed by cervical decapitation. Brains were taken out quickly, washed in ice-cold saline and dissected for CS region following a standard procedure (Glowinski and Iversen 1966). Brain regions were processed immediately for the estimation of OS-related parameters, neurotransmitters and silica content. Behavioural studies were carried out as per plan after 90 days of treatment. Rats in Group II were used to assess spontaneous locomotor activity, 24 h after the last dose of treatment. The same set of rats were used to measure grip strength, 1 h after the spontaneous locomotor activity test. Rotarod test was carried out in Group III. After rotarod test, rats were sacrificed as described above. The half of the CS region of same set of rats was processed immediately for the assay of parameters related with OS, and remaining half of the CS region was kept frozen at −20 °C for the assay of dopamine (DA)-D2 receptors and neurotransmitters and processed within 72 h. Moreover, half of the CS region of individual rats of Group IV was analysed for

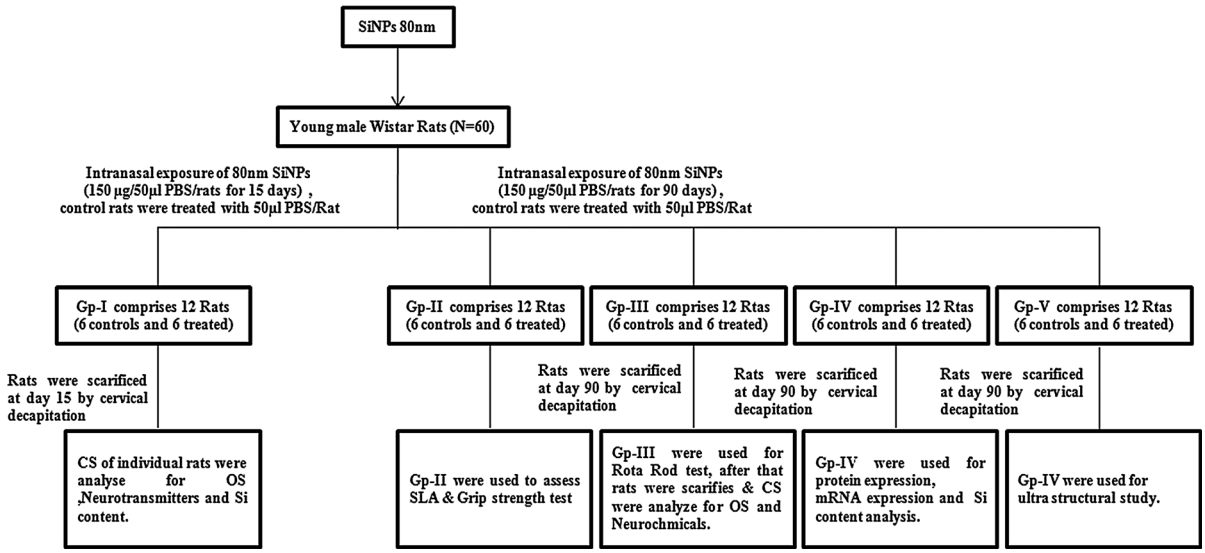

Fig. 1 Experimental design for in vivo experiments

protein and mRNA expression, and remaining half CS region was used for the estimation of silica content. Group V rats were perfused with Karnovsky's fixative, and CS region of perfused rats brain was used for the ultrastructural studies (Fig. 1).

Spontaneous locomotor activity

Spontaneous locomotor activity in rats was assessed using computerized Actimot (TSE, Germany), following the method as described by Yadav et al. (2009). Effect on different parameters including total distance travelled, resting time, stereotypic time, time moving and rearing were studied in controls and treated groups.

Rotarod performance

Effect of SiNPs on motor coordination was studied in rats using Rotomex (Columbus Instruments, USA), and the time of fall from the rotating rod was monitored following the standard procedure of Yadav et al. (2009).

Grip strength

A computerized grip strength metre (TSE, Germany) was used to measure the forelimb grip strength in controls and treated rats following the standard procedure described by Yadav et al. (2009).

Silica nanoparticles content analysis

CS region was removed from treated and control rats and stored at −80 °C. CS region was thawed on the day of analysis. Generally, 0.1 g of the tissue was weighed, digested and analysed for silica content using Inductively Coupled Plasma Optical Emission Spectrometer (ICP-OES, Perkin Elmer.).

Lipid peroxide levels

Lipid peroxide levels, as a measure of malondialdehyde (MDA) formation, were estimated following the method of Ohkawa et al. (1979), and the intensity of pink colour formed during the reaction was read at 532 nm. The values were expressed as µmol MDA/mg protein.

Protein carbonyl

Protein carbonyl content in the CS region of the rat brain was measured following the method of Levine et al. (1990), using 2,4-dinitrophenylhydrazine (DNPH) as a substrate. The difference in absorbance between the DNPH-treated and the HCl-treated samples was determined spectrophotometrically at 375 nm, and the amount of carbonyl contents was

calculated using a molar extinction coefficient (e) of 22.0 mM^{-1} cm^{-1} for aliphatic hydrazones. The values were expressed as nmol/mg protein.

Reduced glutathione

Reduced glutathione (GSH) levels in CS were measured spectrophotometrically, using 5, 5′-dithiobis (2-nitrobenzoic acid) (DTNB) as the colour reagent, following the method of Hasan and Haider (1989). A range of glutathione (2–10 μg) was also run in parallel to plot the standard curve. The values were expressed as μg GSH/g tissue weight.

Superoxide dismutase

Activity of superoxide dismutase (SOD) was assayed following the method of Kakkar et al. (1984) using NADH as a substrate in the post-mitochondrial fraction of CS. The SOD activity was expressed in units/min/mg protein.

Catalase

Activity of catalase in the CS region of the rat brain was assayed following the method of Aebi (1984), spectrophotometrically in the post-mitochondrial fraction using hydrogen peroxide (H_2O_2) as substrate. The activity was expressed in μmol/min/mg protein.

Glutathione peroxidase

Glutathione peroxidase (GPx) activity in CS was measured following the procedure of Flohe and Gunzler (1984). The values were expressed as nmol GSH oxidised/mg protein.

H_2O_2 and O_2^-

The detection of hydroperoxide (H_2O_2) contents in the CS tissue was carried out by the xylenol orange assay, following the method of Nourooz-Zadeh et al. (1994). Superoxide anions (O_2^-) in CS tissue were measured by determining the reduction of 3-{1 [(phenylamino) carbonyl]-3,4-tetrazolium}-bis(4-methoxy-6-nitro) benzenesulfonic acid hydrate (XTT) as described by Oliveira et al. (2001). The values are expressed were nmol/mg tissue.

Assay for catecholamine's

Dopamine (DA), 3,4-dihydroxyphenylacetic acid (DOPAC) and homovanillic acid (HVA) were analysed using high-performance liquid chromatography with electrochemical detector (HPLC ECD) following the method of Kim et al. (1987). The CS tissues were homogenized in 0.1 M perchloric acid containing DHBA, an internal standard at a final concentration of 25 ng/ml. After that the samples were centrifuged at 12,000×g for 5 min. The supernatant was further filtered through 0.25 μm nylon filters before injecting into the HPLC injection pump. A water standard system consisting of a high-pressure isocratic pump, 20-μl sample injector valve, C18 reverse phase column and electrochemical detector was used. Data were recorded and analysed with the help of Breeze software. Mobile phase consisted of 0.15 M NaH_2PO_4, 0.25 mM EDTA, 2 % isopropanol and 1.75 mM sodium octyl sulphate and 4 % methanol, pH of the mobile phase, was adjusted to 4.0. Electrochemical conditions for the experiment were +0.800 V, and sensitivity range was 2 nA. Separation was carried out at a flow rate of 1.2 ml/min. Results were expressed in terms of ng/g wet tissue weight.

Assay for dopamine-D2 receptors

Radioligand receptor binding technique was employed to assay dopamine (DA) D2 receptors in crude synaptic membranes of CS following the standard procedure described in detail by Khanna et al. (1994). ^{3}H-spiperone (18.5 Ci/mmol, 1×10^{-9} M, Perkin Elmer, USA) was used as a radioligand, while haloperidol (1×10^{-6} M) was used as a competitor to assess the extent of non-specific binding. Specific binding was expressed as pmol ligand bound/g protein. Scatchard analysis was carried out at varying concentrations of ^{3}H-spiperone ($0.1–4 \times 10^{-9}$ M) to ascertain whether change in the binding is due to alteration in the affinity (K_d) or number of receptor binding sites (B_{max}).

Real-time PCR

RNA was isolated from control and treated rats using RNAqueous kit (Ambion Inc., Austin, TX, USA), following the manufacturer's protocol. RevertAid^{TM} First Strand cDNA Synthesis kit (Fermentas, St. Leon-

Rot, Germany) was used to synthesize cDNA from 100 ng of RNA. Real-time PCR was performed using Power SYBR green PCR master mix (Applied Biosystems, Foster City, CA, USA) in ABI 7500 Fast Real-Time PCR System (Applied Biosystems, Foster City, CA, USA) following the fast thermal cycling conditions: 95 °C for 5 min and 40 cycles of 95 °C for 15 s and 60 °C for 1 min. Expression levels of Bax, Bcl2, cytochrome *c*, p53 and CHOP were calculated relative to glyceraldehyde 3-phosphate dehydrogenase (GAPDH) as endogenous control. Primers for real-time PCR are given in Table 4.

Isolation of total protein and cytosolic protein from corpus striatum

Total protein was isolated by the method of Yadav et al. (2009). Briefly, the brain CS regions were homogenized in RIPA buffer containing Tris–HCl (50 mM, pH 6.8), NaCl (150 mM), sodium deoxycholate (0.5 %), SDS (0.1 %), protease inhibitor and Triton X-100 (1 %), and centrifuged at 12,000×*g* for 15 min at 4 °C to remove insoluble materials. The pellets were discarded and supernatant contained total protein was used in immunoblot experiment. The cytosolic fractions were prepared by the method of Tang et al. (1998). Protein content was quantified using Lowry et al. (1951).

Immunoblot analysis

Forty microgram of protein sample was separated on 10 % SDS–polyacrylamide gel electrophoresis and electro-blotted on PVDF membrane. The membrane was incubated for 2 h with specific polyclonal IgG antibodies of Bax, Bcl_2, Cyt *c* (Santa Cruz Biotechnology, Inc.), caspase-12, caspase-3, p53, Gadd153/CHOP and β-actin (Abcam), and with respective HRP-conjugated secondary antibodies for 1 h at room temperature. Immunoblot was revealed using Immobilon™ Western Chemiluminescent HRP substrate kit. (Millipore, Corporation, MA, USA). *β*-Actin was used as internal standard. PageRuler™ Prestained Protein Ladder (5 µl) (Thermo, EU) was used to determine molecular weight of the protein bands. Densitometry of the bands obtained was done using NIH software Image J version 1.41 (USA). Band areas were calculated by densitometric scanning and results expressed as Arbitrary Units for each experimental band.

Caspases activity

Enzymatic activities of caspase-3 and caspase-12 were measured using Caspase-3 Colorimetric Assay Kit, and caspase-12 Fluorimetric Assay Kit (BioVision, Inc., Mountain View, CA, USA), respectively, according to manufacturer's instruction. The absorbance was measured at 405 nm for caspase-3, while for caspase-12 fluorescence was recorded at 505 nm emission with 400 nm excitation filter in a SYNERGY-HT multiwell plate reader, Bio-Tek (Winooski, USA).

Electron microscopic study

Ultrastructural changes in CS region of the rat brain were assessed using standard electron microscopic technique. The rats were anesthetized with nembutol (sodium pentobarbitol) solution, 50 mg/kg b.w. and perfused through heart with Karnovsky's fixative (0.1 M paraformaldehyde and glutaraldehyde solution in cacodylate buffer, pH 7.3) following the standard procedure described by (). The brains were quickly removed from the cranium, placed on ice and CS was dissected out. Small pieces of 2–3 mm size were immersed in the same fixative for 4 h and there after washed with 0.1 M cacodylate buffer (pH 7.3). The samples were post fixed for 3 h at 4 °C in 1 % osmium tetroxide prepared in 0.1 M cacodylate buffer. The specimen were washed with distilled water and left in 1 % aqueous uranyl acetate overnight. Subsequently, dehydration was carried out in ascending grades of alcohol, acetone and in pure acetone. Following dehydration, the specimens were embedded in Epon 812 at room temperature. Sections were cut on an LKB-ultramicrotome with a glass knife. Thereafter, sections were mounted on 300 mesh copper grids, stained with 1 % uranyl acetate and lead citrate and examined with a FEI Tecnai G2 Spirit Twin, Czech Republic Transmission Electron TNH Microscope.

Statistical analysis

Statistical analysis was carried out using GraphPad Prism software. The data were analysed using one-way analysis of variance (ANOVA) followed by Newman–Keuls test to compare all pair of columns.

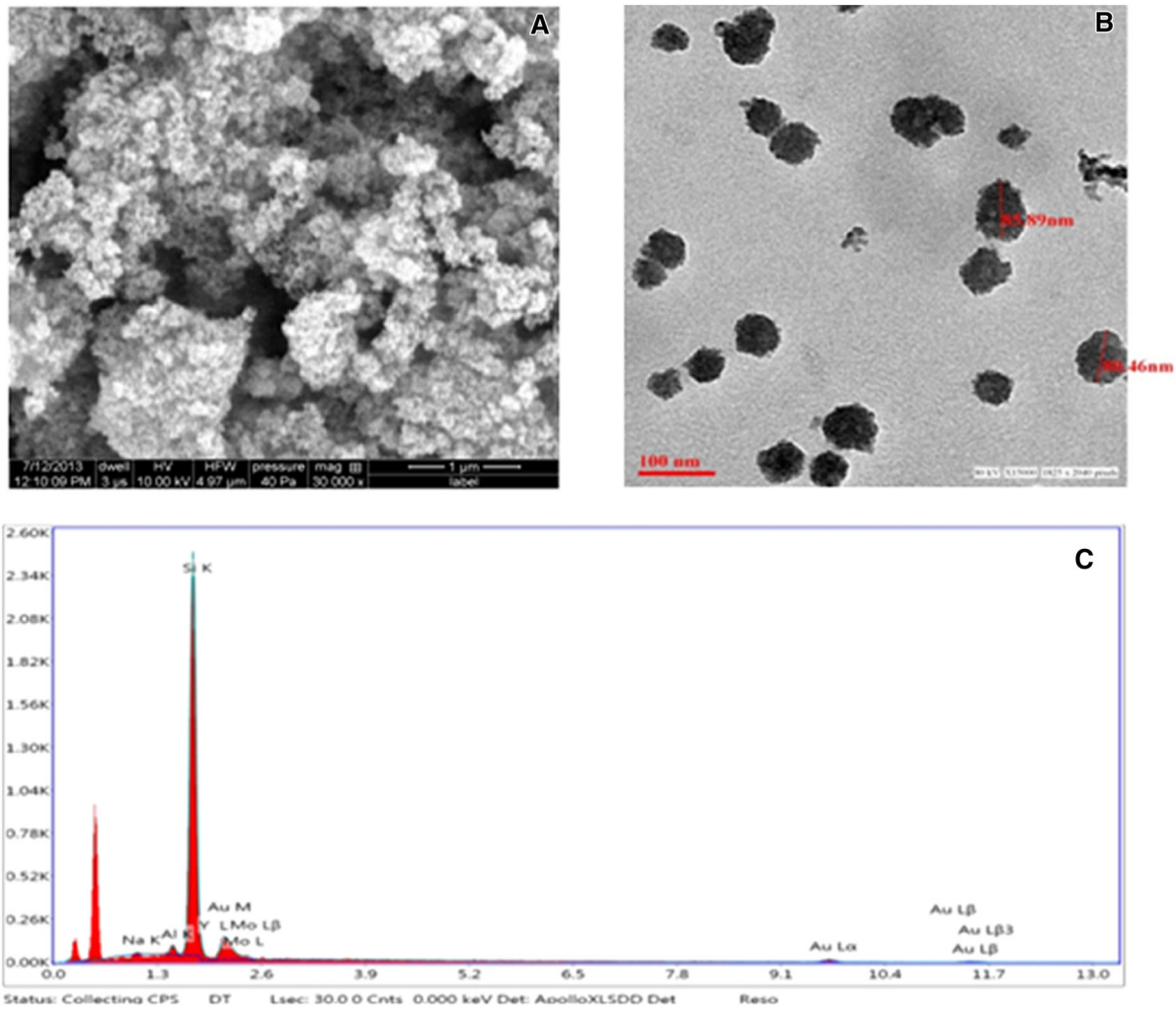

Fig. 2 Characterization of SiNPs (**A**) field emission scanning electron microscope image, (**B**) field emission transmission electron microscope image and (**C**) energy-dispersive X-ray spectrum

Values were expressed as mean ± SEM, and values up to $p < 0.05$ were considered significant.

Results

SiNPs characterization

The results of SEM and TEM indicated that SiNPs having smooth surface and the primary sizes of the SiNPs were about 80 ± 6 nm, and the shapes of the SiNPs were near spherical (Fig. 2A-C). The hydrodynamic size and zeta potential of SiNPs in physiological saline were examined by DLS, which provide quantitative information on stability of the particles during experiment, and results showed that the average hydrodynamic size of SiNPs in physiological saline solution was 397 ± 0.9 nm (Table 1B). Further, zeta potential of SiNPs in physiological saline solution was −25 mV.

SiNPs altered neuromuscular coordination and spontaneous locomotor activity

The rotarod test and grip strength revealed a marked impairment in the muscle strength and coordination in SiNPs-treated group after 90 days exposure with

respect to control group. The average retention time was reduced by 54.61 % in treated group when compared to the controls (Table 2A). The treated animals showed neuromuscular incoordination and seemed confused during training period as compared to the control animals. None of the SiNPs-treated animals could maintain themselves on the rotating rod for the full quota of the cut off time (180 s). Forelimb grip strength was also found to be significantly decreased in treated rats (56.6 %), compared to controls (Table 2B). A significant decrease in total distance travelled (65 %), time moving (39.8 %), rearing (52 %) and an increase in resting time (14.2 %) was observed in treated rats with respect to control group (Table 2C).

Accumulation of SiNPs in corpus striatum

The first and most important step in assessing the neurotoxicity of nanoparticles is to determine their fate in the brain. In the present study, no significant increase in SiNPs content in CS was observed on day 15. However, intranasal instillation of SiNPs for 90 days resulted in a significant increase in SiNPs content in CS, when compared with the controls (Fig. 3).

SiNPs induce oxidative stress and disturbs antioxidant defence in corpus striatum

We found significant increase (118 %) in lipid peroxide levels and protein carbonyl formation (74.2 %) in treated group, when compared with the controls (Fig. 4C,D). Moreover, SiNPs significantly increased the production rate of H_2O_2 (100.8 %) and O_2^- (91.4 %), in CS of treated rats as compared with controls (Fig. 4A,B). We also examined the levels of antioxidants like MnSOD, CAT, glutathione reductase and reduced glutathione and found significant decrease in MnSOD (51.2 %), CAT (50 %), glutathione reductase (28.13 %) and reduced glutathione (41.06 %) in CS of SiNPs administrated rats, when compared with control group (Figs. 5A-D).

SiNPs perturbed catecholamine levels and dopamine D2 receptor in corpus striatum

The levels of DA, DOPAC and HVA were significantly reduced in CS of SiNPs-treated rats. We found significant reduction in the levels of DA (56.6 %), DOPAC (40.3 %) and HVA (49.9 %) in treated rats, as compared with controls (Fig. 6A). Radioligand binding assay showed significant decrease in the binding of ^{3}H-spiperone to striatal membranes, known to label dopamine receptors (34.3 %) in SiNPs-treated

Table 2 Changes in motor coordination and neurobehavioral impairment in rats, following exposure to SiNPs for 90 days

Parameter	Control group	SiNPs-treated group
A		
Rota rot	269 ± 20	122 ± 12*
B		
Grip strength	786 ± 34	341 ± 29*
C		
Total distance	6508 ± 877.0	2245 ± 887**
Resting time	196 ± 15.65	224.8 ± 25.15*
Time moving	118 ± 4.05	71.17 + 23.0*
Stereotypictime	104.5 ± 18.3	96.5 ± 10.3
Time rearing	23 ± 9.19	11 ± 5.21*

(A) Rotarod test, (B) Forelimb grip strength and (C) Different parameters of locomotor activity in rats following exposure to SiNPs at post instillation of day 90. Data were analysed by one-way analysis of variance followed by Newman–Keuls test. Values are mean ± SEM of six animals in each group

The asterisk indicates the significant difference between treated and control groups (* $p < 0.05$ and ** $p < 0.01$)

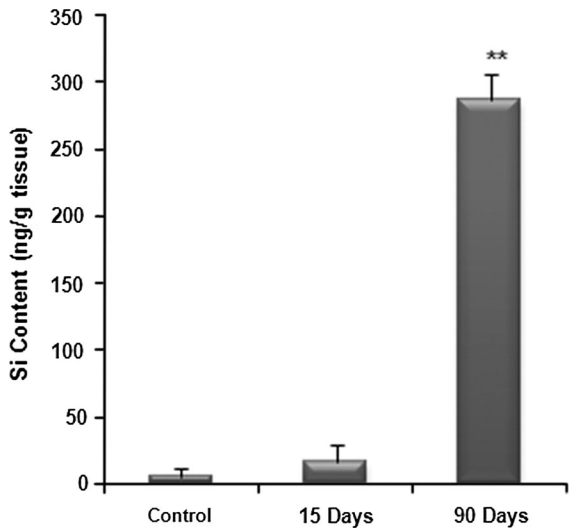

Fig. 3 Si content in CS of rat brains ($n = 6$) after intranasal instillation with SiNPs at time points of 15 and 90 days. **$p < 0.01$ when compared with control groups

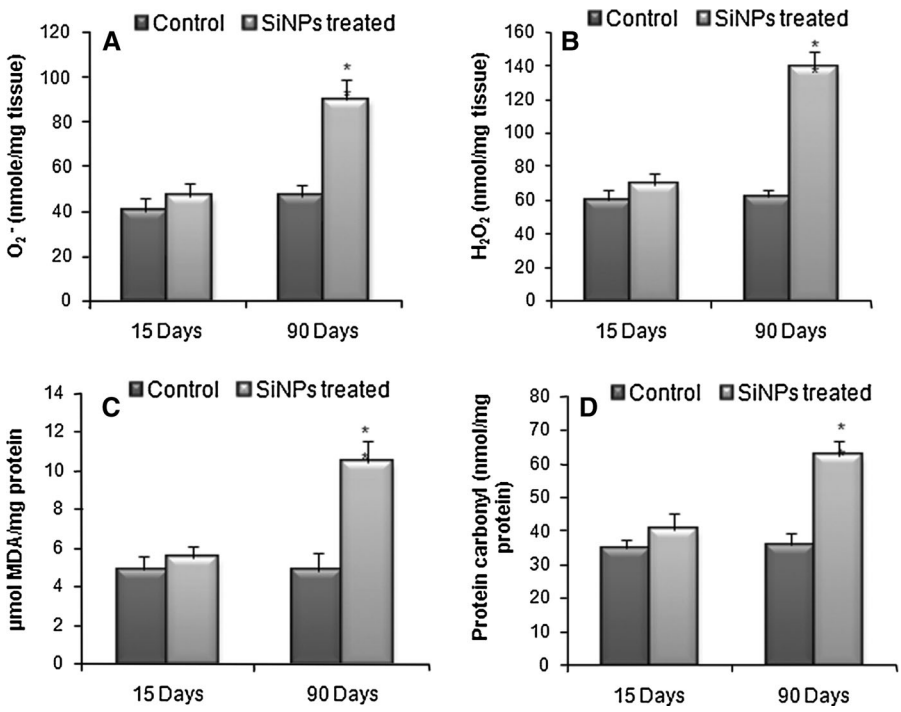

Fig. 4 Changes in H_2O_2, O_2^-, MDA level and Protein carbonyl levels in the CS of rats ($n = 6$) intranasally instilled with physiological saline and SiNPs at the time point of 15 and 90 days. (**A**,**B**,**C** and **D**) H_2O_2, O_2^-, MDA level and protein carbonyl content in the CS. Data were analysed by one-way analysis of variance followed by Newman–Keuls test. Values are mean ± SEM of six animals in each group. The *asterisk* indicates the significant difference between treated and control groups (*$p < 0.05$)

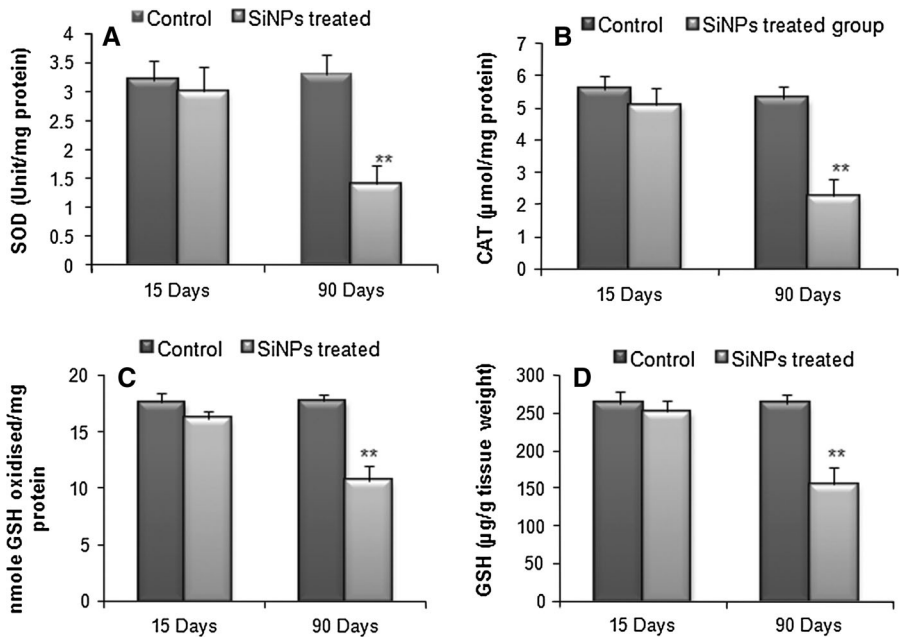

Fig. 5 Levels of SOD, CAT, GSH and GPx levels in the CS of rats ($n = 6$) intranasally instilled with physiological saline and SiNPs at the time point of 15 and 90 days. (**A**-**D**) SOD, CAT, GSH and GPx levels in CS. Data were analysed by one-way analysis of variance followed by Newman–Keuls test. Values are mean ± SEM of six animals in each group. The *asterisk* indicates the significant difference between treated and control groups (**$p < 0.01$)

rats, when compared with controls (Fig. 6B). Scatchard analysis revealed that the decrease in the binding was due to decrease in the number of binding sites (B_{max}), and no significant effect on affinity (K_d) was found in the SiNPs-treated rats, when compared with the control group (Table 3).

SiNPs-induced mitochondrial and ER stress-mediated apoptosis in corpus striatum

To confirm whether chronic exposure of SiNPs play any role in neurodegeration, we analysed expression of apoptosis-related proteins (Bax, Bcl-2, cytochrome

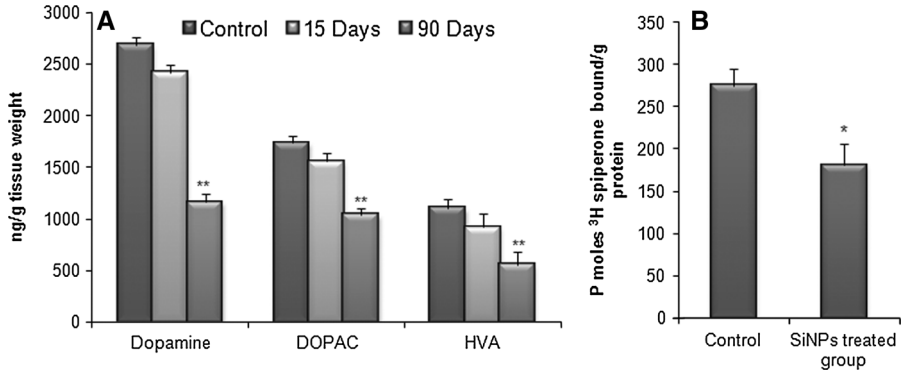

Fig. 6 Changes of (**A**) DA, DOPAC and HVA level in the CS of rats ($n = 6$) after intranasal exposure of SiNPs at the time point of 15 and 90 days, and (**B**) Dopamine D2 receptors at post instillation of 90 days. Data were analysed by one-way analysis of variance followed by Newman–Keuls test. Values are mean ± SEM of six animals in each group. The *asterisk* indicates the significant difference between treated and control groups (*$p < 0.05$ and **$p < 0.01$)

Table 3 Scatchard analysis of ^{3}H-Spiperone to CS membranes of rats following exposure to SiNPs for 90 days

Parameter	Control	SiNP Treated
K_d	1.84 ± 0.12	1.62 ± 0.13
B_{max}	565 ± 49	226 ± 25**

Values are mean ± SEM of six animals in each group. The asterisk indicates the significant difference between treated and control groups (** $p < 0.01$). K_d is the dissociation constant expressed in nM, B_{max} is the maximum number of binding sites expressed in Pico moles ^{3}H-Spiperone bound/g protein

c, caspase-3, p53, caspase-12 and CHOP) by western blotting and m-RNA expression of Bax, Bcl-2, CHOP and p53 by real-time PCR. The protein and m-RNA expression of pro-apoptotic protein Bax was found to be increased, while antiapoptotic protein Bcl-2 showed downregulation (Fig. 7A,D) in CS of treated rats. Immunoblotting of cytochrome *c* revealed a single protein band in cytosolic fractions of CS of treated rats, which confirms the release of cytochrome *c* from mitochondria to cytosol (Fig. 7B). Immunoblotting and enzymatic activity of caspase-3 revealed that subchronic SiNPs exposure caused significant increase in caspase-3 in CS of treated rat with respect to controls (Fig. 7A,E). These findings confirm that cytochrome *c* release and subsequent activation of caspase-3 may form an essential component of neuronal degeneration in chronic form of SiNPs neurotoxicity. Further, we demonstrated the expression of p53 and found that p53 protein and m-RNA levels were upregulated (Fig. 7A,D) in CS of treated rats with respect to controls. ER stress-related marker CHOP/GADD153 and caspase 12 were significantly increased in CS of treated rats (Fig. 7C, F), when compared with the controls.

SiNPs-induced ultrastructural changes in corpus striatum

To provide further insight into the nature of the neuronal cell death caused by SiNPs, we examined the CS tissue for ultrastructural changes by transmission electron microscopy (Fig. 8A-D). The electron microscopic studies depicted intensely electron dense mitochondria, mitochondrial swelling, loss of mitochondria cristae, changes in nuclear shape, chromatin condensation, dilation of rough endoplasmic reticulum, increase in lysosomes and degeneration of neurodendron in CS of treated rats.

Discussion

Physicochemical properties such as particle size, zeta potential and hydrodynamic size are important parameters to assess the toxic effects of nanomaterials (Jiang et al. 2009; Murdock et al. 2008). In the present study, characterization of SiNPs was carried out by SEM and TEM, which showed that nanoparticles were almost spherical in shape, smooth surface, well dispersed and with an average diameter of 80 ± 8 nm (Fig. 2A,B). We observed that the hydrodynamic size of SiNPs, measured by DLS, was approximately 4–5 times

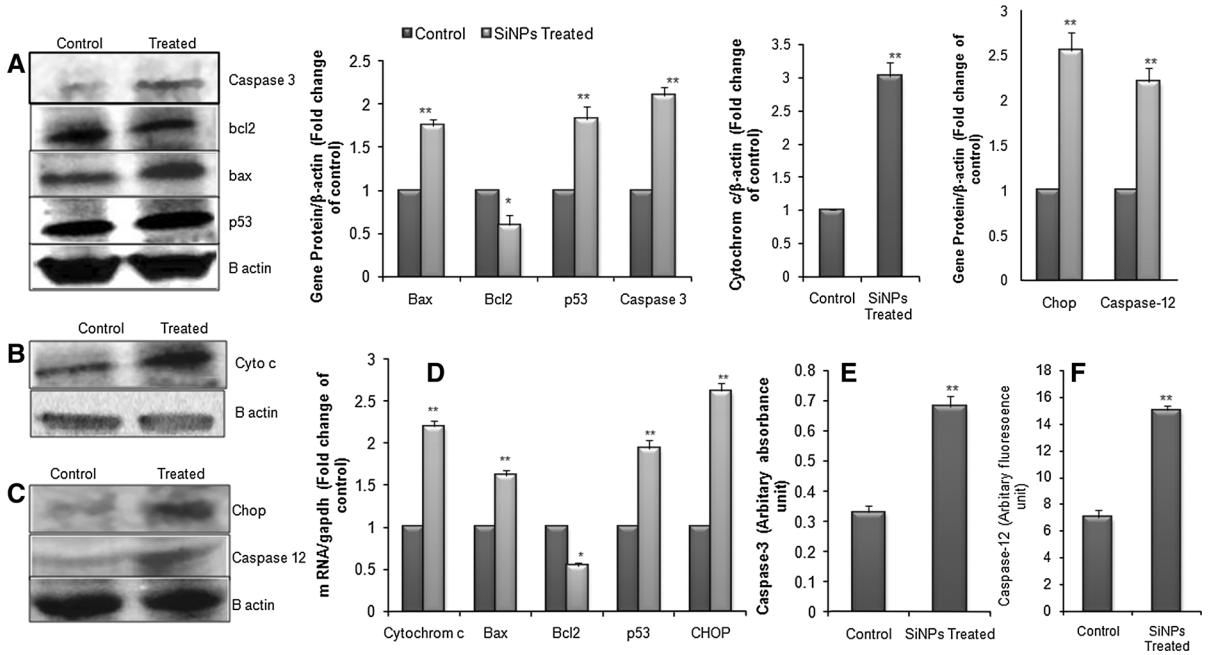

Fig. 7 SiNPs induces mitochondrial and ER stress-mediated apoptosis in CS of rat brain at post instillation of day 90. (**A**–**C**) Western blot analysis of p53, bax, bcl-2, cytochrome *c*, caspase-3, caspase-12 and CHOP. Results were normalized to *β*-actin (**D**) mRNA levels of Bax, Bcl2, p53, cytochrome *c* and CHOP were determined by real-time PCR, endogenous control was GAPDH (**E**, **F**) caspase 3 and caspase 12 activity. Data from mean ± SEM of three independent experiments. The *asterisk* indicates the significant difference between treated and control groups (*$p < 0.05$, **$p < 0.01$)

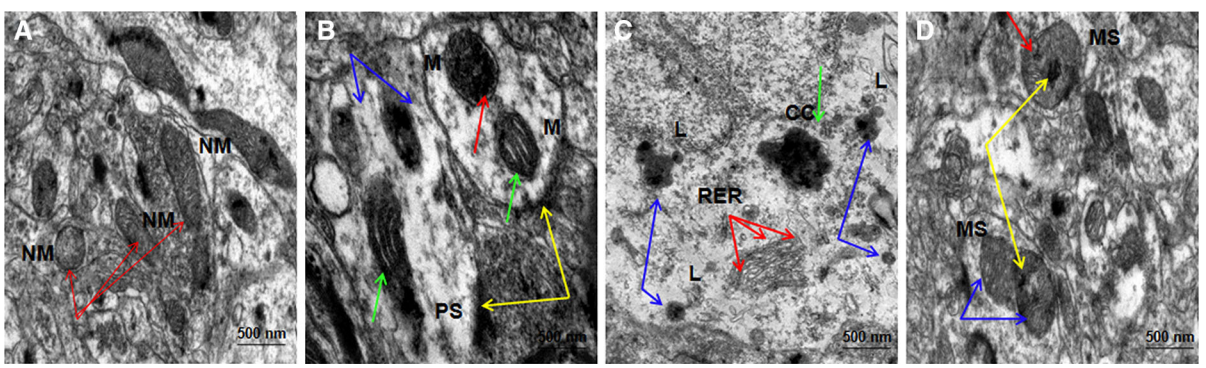

Fig. 8 Transmission electron micrograph of CS showing apoptotic morphology after subchronic SiNPs exposure for 90 days. (**A**) Control rat showing normal mitochondria (*red arrow*) *NM* normal mitochondria; magnification ×15,000. (**B**) Electron micrograph of SiNPs-treated rat brain CS exhibit part of an axonal profile showing two mitochondria, depicted longitudinal cristae which are electron lucent (*green arrow*); one mitochondrion at the top (*red arrow*) shows transverse cristae with electron dense matrix. Some particles are present in the mitochondrion (*blue arrow*). Curved perforated synapse seen at the bottom (*yellow arrow*). *M* Mitochondria, *PS* perforated synapse, magnification ×20,000. (**C**) Change in nuclear shape and chromatin condensation (*green arrow*), slight dilation of rough endoplasmic reticulum clearly seen (*red arrow*) and increases in lysosome were observed in CS of treated rat. *CC* Chromatin condensation, *RER* rough endoplasmic reticulum, *L* lysosome, magnification ×15,000. (**D**) Mitochondria underwent morphological changes such as matrix swelling, loss of mitochondrial cristae (*red arrow*), mitochondrial swelling (*blue arrow*) and some particles were seen inside the mitochondria (*yellow arrow*). *MS* Mitochondria swelling, magnification ×15,000. (Color figure online)

higher (i.e. 397 ± 12 nm) than that calculated by TEM (80 ± 8 nm). The higher size of SiNPs in aqueous suspension, as compared to TEM size, may be due to the tendency of particles to agglomerate in aqueous state. Our results are consistent with previous reports (Liu et al. 2010; Liu and Sun 2010). Moreover, agglomeration of particles depends on the surface charge. The surface charge of SiNPs, determined as zeta potential, was −25 mV in PBS. Our results showed that the SiNPs possessed uniform shape and structure along with relatively uniform dispersibility, which are important factors for nanotoxicity studies.

There is paucity of awareness about the potential adverse effects of SiNPs on brain function, as also regarding the relationship between inhalation exposure of SiNPs with the onset of neurodegenerative disorders. The present study mainly focused on investigating the effect of subchronic inhalation exposure to SiNPs on CS of rat brain. The CS is responsible for regulating autokinetic stability, muscular tension and posture. Moreover, neuronal damage to the CS is reported to be closely correlated with Parkinson's disease (Bugiani et al. 1980; Pitcher et al. 2012; Sterling et al. 2013). Our findings are noteworthy as CS appears to be the major site of intranasally instilled SiNPs accumulation (Fig. 3). Our results showed that approximately 50 % of the nanoparticles remained in the CS of the exposed rats. The high surface to volume ratio of nanoparticles deposited in brain for prolonged period may contribute to cellular interaction and free radical production, and these reactions may lead to brain damage and increase the risk of developing neurodegenerative disorders (Wu et al. 2011a, b).

The results of the present study demonstrated that SiNPs have potential to cause oxidative injuries, as we observed increased levels of H_2O_2 and O_2^- in OS (Fig. 4A,B). H_2O_2 and O_2^- have traditionally been regarded as a by-product of ROS and have been implicated in transcription factor activation and are also reported to play a role in neurodegenerative diseases (Hu et al. 2011). Peroxidation of membrane lipids may be one of the mechanisms by which ROS contribute to the cascade of events leading to damage of cell membrane and intracellular cytoplasmic bodies. Therefore, the observed elevated MDA levels (Fig. 4C) may be associated with membrane dysfunction and triggering events leading to neuronal injury. We also checked protein carbonyl formation, as an index of protein oxidation, and indeed it was found to be significantly elevated in CS of treated rats (Fig. 4D). It has been suggested that oxidatively modified proteins accumulate in various conditions of OS such as ischaemia reperfusion, Parkinson's and Alzheimer's disease, etc. (Barbara and Earl 1997).

From our results, it was also evident that SiNPs caused redox imbalance in CS through the marked depletion in GSH, CAT, SOD and GRx levels (Fig. 5A-D). These enzymes and GSH are considered to be the first line of defence against deleterious effects of ROS (Wang et al. 2009a, b). These data clearly indicate the adverse biological effects of SiNPs exposure on CS of rat brain, and this may ultimately enhance the risk of SiNPs-related neurotoxicity.

To check the OS-mediated neurological damage, we also assessed the levels of DA and its metabolites, and found significant reduction in DA, DOPAC and HVA levels in the CS of treated animals (Fig. 6A). Furthermore, it may be pointed out here that there are reports of an intimate relationship between DA metabolism and ROS generation. The oxidative deamination of catecholamines by monoamine oxidase (MAO) generates hydrogen peroxide, which in turn may lead to OS in catecholaminergic neurons or catecholamine degrading cells (Sulzer et al. 2000; Meiser et al. 2013). In contrast, non-enzymatical and spontaneous auto-oxidation of DA produces O_2^- and reactive quinines. Both quinones and ROS can react unspecifically with many cellular components altering their functionality and thus being potentially neurodegenerative (Graham 1978; Napolitano et al. 2011). Earlier reports have shown that dopaminergic system is involved in many psychiatric and neurological disorders, including Parkinson's disease (Meiser et al. 2013; Shafer et al. 2005).

We also report decrease in dopamine-D2 receptors in CS, as reflected by a decrease in the binding of ^{3}H-spiperon to striatal membranes (Fig. 6B; Table 3). At present, it is difficult to explain the exact reason for decreased binding of dopamine-D2 receptors. It may either be due to excessive dopaminergic neuronal cell death, as a result of redox imbalance, or decreased levels of dopamine, which may influence the sensitivity of their receptors in the striatum. It may also be a result of direct interaction of SiNPs with dopamine receptors, leading to decreased binding, as there are numerous reports of a number of nanoparticles interacting with the receptors directly (Wang et al.

Table 4 Primers for real-time PCR

CHOP	F 5′-CAC CTC CCA AAG CCC TCG CTC TC-3′
	R 5′-TCA TGC TTG GTG CAG ACT GAC CAT-3′
Bax	F 5′-ACACCTGAGCTGACCTTG-3′
	R 5′-AGCCCATGATGGTTCTGATC-3′
Bcl-2	F 5′-CATGCGACCTCTGTTTGA-3′
	R 5′-GTTTCATGGTCCATCCTTG-3′
p53	F 5′-CTACTAAGGTCGTGAGACGC TGCC-3′
	R 5′-TCAGCATACAGGsTTTCCT TCCACC-3′
Cytochrome *C*	F 5′-TAAATATGAGGGTGTCGC-3′
	R 5′-AAGAATAGTTCCGTCCTG-3′
GAPDH	F 5′-GTC TAC TGG CGT CTT CAC CA-3′
	R 5′-GTG GCA GTG ATG GCA TGG AC-3′

2009a, b; Bartczak et al. 2011; Vacha et al. 2012). Role of dopamine and its receptors in modulating the motor behaviour is well known (Yadav et al. 2009). We also found decrease in distance travelled associated with resting time in rats exposed to SiNPs. This indicates impaired motor performance. Furthermore, decrease in grip strength and rotarod performance showed impaired motor coordination. These changes may be associated with the decrease in the sensitivity of dopamine receptors in CS of treated rats (Table 4).

To explore the possible molecular mechanism of SiNPs-induced neuronal apoptosis in CS, the expression level of several regulators involved in apoptosis was assessed. It was observed that nanoparticles disturbed intracellular redox homeostasis which resulted in the generation of ROS (Wang et al. 2009a, b). ROS may trigger OS in mitochondria and ER, which, under adverse conditions, result into the promotion of stress-mediated apoptosis (Liu and Sun 2010; Chen et al. 2008; Wu et al. 2011a, b). Our results revealed that SiNPs disturbed bax/bcl2 ratio (Fig. 7A,D) in CS, and this was confirmed by the release of cytochrome *C* (Fig. 7C) from the mitochondrial membrane and activation of executioner caspase 3, which is a hallmark of apoptosis cascade (Fig. 7E). Furthermore, we found that these effects were p53 mediated. It is generally believed that OS activates multiple signalling pathways, including the p53 signal transduction pathway (Circu and Aw 2010). Results showed that p53 protein as well as its mRNA level was upregulated in CS with respect to controls. ER stress is implicated in many neurological disorders (Yoshida 2007) and is also closely linked to OS and mitochondrial damage (Deniaud et al. 2008; Li et al. 2010). Therefore, the role of ER stress in SiNPs-induced apoptosis was examined. CHOP/GADD153 and activated caspase-12 are the sensor of ER stress, beside this apoptosis-related proteins like bax and bcl2 also reside in ER (Nozaki et al. 2001; Momoi 2004). Our results clearly indicated that caspase-12 activation together (Fig. 7C,F) with enhanced CHOP/GADD153 expression in CS (Fig. 7C) of SiNPs-treated rats can be linked with disruption in bax/bcl2 homeostasis and redox imbalance (Barone et al. 1994; Matsumoto et al. 1996). Moreover, our results also suggest that SiNPs may promote the perturbation in the mitochondrial and ER function in the CS of rat brain which in turn may result in the activation of apoptotic proteins in these organelles, and thereby promotes apoptosis (Fig. 8A-D). Furthermore, the ultrastructural changes in CS of SiNPs-treated rat brain revealed that mitochondria and ER underwent various morphological changes such as mitochondrial swelling, electron dense mitochondria and dilation in rough endoplasmic reticulum. The changes observed in electron microscopic studies provided clear evidence that SiNPs-induced morphological changes were consistent with our results of apoptotic neuronal cell death.

Conclusion

The results of the present study demonstrated that intranasally instilled SiNPs were deposited in CS region of rat brain. The accumulation of SiNPs resulted in OS, due to the increased formation of ROS and depletion of cellular antioxidants. Furthermore, we also observed SiNPs-induced apoptosis, which was mediated by mitochondrial as well as ER stress signalling pathways. The generation of OS and neuronal apoptotic cell death may constitute the intervening biochemical steps between subchronic exposure to SiNPs and perturbation in neurochemical parameters and appearance of various neurobehavioural deficits. Our results clearly demonstrated the potential neurotoxicity of SiNPs and their possible role in neurodegenerative disorders. However, further studies are needed to gain a better understanding of

memory functions and nanoparticles-induced apoptosis, by the activation of unfolded protein responses (UPR), particularly in ER stress.

Acknowledgments We gratefully acknowledge the financial support received from Council of Science & Technology U. P. for carrying out the study.

Conflict of interest The authors declare that they have no conflict of interest.

References

Aebi H (1984) Catalase in vitro. In: Packer L (ed) Methods in enzymology, vol 105. Academic Press, New York, pp 121–126

Barbara SB, Earl RS (1997) Protein oxidation in aging, disease and oxidative stress. J Biol Chem 272:20313–20316

Barone MV, Crozat A, Tabaee A, Philipson L, Ron D (1994) CHOP (GADD153) and its oncogenic variant, TLS-CHOP, have opposing effects on the induction of G1/S arrest. Genes Dev 8:453–464

Bartczak D, Sanchez-Elsner T, Louafi F, Millar TM, Kanaras AG (2011) Receptor-mediated interactions between colloidal gold nanoparticles and human umbilical vein endothelial cells. Small 7:388–394

Bharali DJ, Klejbor I, Stachowiak EK, Dutta P, Roy I, Kaur N, Bergey EJ, Prasad PN, Stachowiak MK (2005) Organically Modified Silica Nanoparticles: a Nonviral Vector for In Vivo Gene Delivery and Expression in the Brain. Proc Natl Acad Sci USA 32:11539–11544

Bottini M, D'Annibale F, Magrini A, Cerignoli F, Arimura Y, Dawson MI, Bergamaschi E, Rosato N, Bergamaschi A, Mustelin T (2007) Quantum dot-doped silica nanoparticles as probes for targeting of T-lymphocytes. Int J Nanomed 2:227–233

Brouwer D (2010) Exposure to manufactured nanoparticles in different workplaces. Toxicology 269:120–127

Bugiani O, Perdelli F, Salvarani S, Leonardi A, Mancardi GL (1980) Loss of striatal neurons in Parkinson's disease: a cytometric study. Eur Neurol 19:339–344

Chen G, Ma C, Bower KA, Shi X, Ke Z, Luo J (2008) Ethanol promotes endoplasmic reticulum stress-induced neuronal death: involvement of oxidative stress. J Neurosci Res 86:937–946

Christen V V, Capelle M, Fent K (2013) Silver nanoparticles induce endoplasmatic reticulum stress response in zebrafish. Toxicol Appl Pharmacol 272:519–528

Circu ML, Aw TY (2010) Reacting oxygen species, cellular redox system and apoptosis. Free Radical Biol Med 6:749–762

Deniaud A, Sharaf el dein O, Maillier E, Poncet D, Kroemer G, Lemaire C, Brenner C (2008) Endoplasmic reticulum stress induces calcium-dependent permeability transition, mitochondrial outer membrane permeabilization and apoptosis. Oncogene 27:285–299

Doyle KM, Kennedy D, Gorman AM, Gupta S, Healy SJ, Samali A (2011) Unfolded proteins and endoplasmic reticulum stress in neurodegenerative disorders. J Cell Mol Med 15:2025–2039

Elder A, Gelein R, Silva V, Feikert T, Opanashuk L, Carter J, Potter R, Maynard A, Ito Y, Finkelstein J, Oberdörster G (2006) Translocation of inhaled ultrafine manganese oxide particles to the central nervous system. Environ Health Perspect 114:1172–1178

Flohe L, Gunzler WA (1984) Assays of glutathione peroxidase. Method Enzymol 105:114–121

Galehdar Z, Swan P, Fuerth B, Callaghan SM, Park DS, Cregan SP (2010) Neuronal apoptosis induced by endoplasmic reticulum stress is regulated by ATF4-CHOP-mediated induction of the Bcl-2 homology 3-only member PUMA. J Neurosci 30:16938–16948

Glowinski J, Iversen LL (1966) Regional studies of catecholamines in the rat brain. The disposition of 3H-norepinephrine 3H-dopamine and 3H-dopa in various regions of the brain. J Neurochem 13:655–659

Graham DG (1978) Oxidative pathways for catecholamines in the genesis of neuromelanin and cytotoxic quinones. Mol Pharmacol 14:633–643

Hasan M, Haider SS (1989) Acetyl homocysteine thiolactone protect against some neurotoxic effects of thallium. Neurotoxicology 10:257–262

Hu R, Zheng L, Zhang T, Gao G, Cui Y, Cheng Z, Cheng J, Hong M, Tang M, Hong F (2011) Molecular mechanism of hippocampal apoptosis of mice following exposure to titanium dioxide nanoparticles. J Hazard Mater 191:32–40

Jiang J, Oberdorster G, Bisw P (2009) Characterization of size, surface charge, and agglomeration state of nanoparticle dispersions for toxicological studies. J Nanopart Res 11:77–89

Kakkar P, Das B, Viswanathan PN (1984) A modified spectrophotometric assay of superoxide dismutase. Indian J Biochem Biophys 21:130–132

Khanna VK, Husain R, Seth PK (1994) Effect of protein malnutrition on the neurobehavioral toxicity of styrene in young rats. J Appl Toxicol 14:351–356

Kim C, Speisky MB, Klarevla SN (1987) Rapid and sensitive method for measuring norepinephrine, dopamine, 5HT and their major metabolites in rat brain by high performance liquid chromatography. J Chromatogr 386:25–35

Kroemer G, Galluzzi L, Brenner C (2007) Mitochondrial membrane permeabilization in cell death. Physiol Rev 87:99–163

Levine RL, Garland D, Oliver CN, Amici A, Climent I, Lenz AG, Ahn BW, Shaltiel S, Stadtman ER (1990) Determination of carbonyl content in oxidatively modified proteins. Methods Enzymol 186:464–478

Li G, Scull C, Ozcan L, Tabas I (2010) NADPH oxidase links endoplasmic reticulum stress, oxidative stress, and PKR activation to induce apoptosis. J Cell Biol 191:1113–1125

Liao CM, Chiang YH, Chio CP (2009) Assessing the airborne titanium dioxide nanoparticles related exposure hazard at workplace. J Hazard Mater 162:57–65

Liu X, Sun J (2010) endothelial cells dysfunction induced by silica nanoparticles through oxidative stress via JNK/P53 and NF-kappaB pathways. Biomaterials 32:8198–8209

Liu S, Xu L, Zhang T, Ren G, Yang Z (2010) Oxidative stress and apoptosis induced by nanosized titanium dioxide in PC12 cells. Toxicology 267:172–177

Lockman PR, Koziara JM, Mumper RJ, Allen DD (2004) Nanoparticle surface charges alter blood–brain barrier integrity and permeability. J Drug Target 12:635–641

Lowry OH, Rosenbrough NJ, Farr AL Randall RJ (1951) Protein measurement with the folin phenol reagent. J Biol Chem 192:265–275

Matsumoto M, Minami M, Takeda K, Sakao Y, Akira S (1996) Ectopic expression of CHOP (GADD153) induces apoptosis in M1 myeloblastic leukemia cells. FEBS Lett 395:143–147

Meiser J, Weindl D, Hiller K (2013) Complexity of dopamine metabolism. Cell Commun Signal 11:34

Momoi T (2004) Caspases involved in ER stress-mediated cell death. J Chem Neuroanat 28:101–105

Murdock RC, Braydich-Stolle L, Schrand AM, Schlager JJ, Hussain SM (2008) Characterization of nanomaterial dispersion in solution prior to in vitro exposure using dynamic light scattering technique. Toxicol Sci 101:239–253

Nakagawa T, Zhu H, Morishima N, Li E, Xu J, Yankner BA, Yuan J (2000) Caspase-12 mediates endoplasmic reticulum-specific apoptosis and cytotoxicity by amyloid-β. Nature 403:98–103

Napolitano A, Manini P, D'Ischia M (2011) Oxidation chemistry of catecholamines and neuronal degeneration: an update. Curr Med Chem 18:1832–1845

Nourooz-Zadeh J, Tajaddini-Sarmadi T, Wolff SP (1994) Measurement of plasma hydroperoxide concentrations by the ferrous oxidation-xylenol orange assay in conjunction with triphenylphosphine. Anal Biochem 220:403–409

Nozaki S, Sledge GW Jr, Nakshatri H (2001) Repression of GADD153/CHOP by NF-kappaB: a possible cellular defense against endoplasmic reticulum stress-induced cell death. Oncogene 20:2178–2185

Ohkawa H, Ohishi N, Yagi K (1979) Assay for lipid peroxides in animal tissues by thiobarbituric acid reaction. Anal Biochem 95:351–358

Oliveira CP, Lopasso FP, Laurindo FR (2001) Protection against liver ischemia–reperfusion injury in rats by silymarin or verapamil. Transplant. Proc 33:3010–3014

Oszlanczi G, Papp A, Szabo A (2011) Nervous system effects in rats on subacute exposure by lead-containing nanoparticles via the airways. Inhal Toxicol 23:173–181

Parveen A, Rizvi SHM, Gupta A, Singh R, Ahmad I, Mahdi F, Mahdi AA, Singh R, Ahmad I, Mahdi F, Mahdi AA (2012) NMR-based metabonomics study of sub-acute hepatotoxicity induced by silica nanoparticles in rats after intranasal exposure. NMR Cell Mol Biol 58(Supp):196–203

Pitcher TL, Melzer TR, Macaskill MR, Graham CF, Livingston L, Keenan RJ, Watts R, Dalrymple-Alford JC, Anderson TJ (2012) Reduced striatal volumes in Parkinson's disease: a magnetic resonance imaging study. Transl Neurodegener. 21:17

Rizvi SHM, Parveen A, Verma AK, Ahmad I, Arshad M, Mahdi AA (2014) Aluminium induced endoplasmic reticulum stress mediated cell death in SHSY5Y neuroblastoma cell line is independent of p53. PLoS ONE 9(5):e98409

Sanges D, Marigo V (2006) Cross-talk between two apoptotic pathways activated by endoplasmic reticulum stress: differential contribution of caspase-12 and AIF. Apoptosis 11:1629–1641

Shafer TJ, Meyer DA, Crofton KM (2005) Developmental neurotoxicity of pyrethroid insecticides: critical review and future research needs. Environ Health Perspect 113:123–136

Slowing II, Trewyn BG, Lin VSY (2007) Mesoporous silica nanoparticles for intracellular delivery of membrane-impermeable proteins. J Am Chem Soc 129:8845–8849

Sterling NW, Du G, Lewis MM, Dimaio C, Kong L, Eslinger PJ, Styner M, Huang X (2013) Striatal shape in Parkinson's disease. Neurobiol Aging 34:2510–2516

Sulzer D, Bogulavsky J, Larsen KE, Behr G, Karatekin E, Kleinman MH, Turro N, Krantz D, Edwards RH, Greene LA, Zecca L (2000) Neuromelanin biosynthesis is driven by excess cytosolic catecholamines not accumulated by synaptic vesicles. Proc Natl Acad Sci USA 97:11869–11874

Takenaka S, Karg E, Roth C, Schulz H, Ziesenis A, Heinzmann U, Schramel P, Heyder J (2001) Pulmonary and systemic distribution of inhaled ultrafine silver particles in rats. Environ Health Perspect 109:547–551

Tang DG, Li L, Zhu Z, Joshi B (1998) Apoptosis in the absence of cytochrome *c* accumulation in the cytosol. Biochem. Biophys Res 242:380–384

Vacha R, Martinez-Veracoechea FJ, Frenkel D (2012) Intracellular release of endocytosed nanoparticles upon a change of ligand–receptor interaction. ACS Nano 6:10598–10605

Walter L, Hajnoczky G (2005) Mitochondria and endoplasmic reticulum: the lethal interorganelle cross-talk. J Bioenerg Biomembr 37:191–206

Wang J, Liu Y, Jiao F, Lao F, Li W, Gu Y, Li Y, Ge C, Zhou G, Li B, Zhao Y, Chai Z, Chen C (2008) Time-dependent translocation and potential impairment on central nervous system by intranasally instilled TiO_2 nanoparticles. Toxicology 254:82–90

Wang B, Feng WY, Zhu MT, Wang Y, Wang M, Gu Y, Ouyang H, Wang H, Li M, Zhao Y, Chai Z, Wang H (2009a) Neurotoxicity of low-dose repeatedly intranasal instillation of nano- and submicron-sized ferric oxide particles in mice. J Nanopart Res 11:41–53

Wang J, Rahman MF, Duhart HM, Newport GD, Patterson TA, Murdock RC, Hussain SM, Schlager JJ, Ali SF (2009b) Expression changes of dopaminergic system-related genes in PC12 cells induced by manganese, silver, or copper nanoparticles. Neurotoxicology 30:926–933

Win Shwe TT, Yamamoto S, Ahmed S, Kakeyama M, Kobayashi T, Fujimaki H (2006) Brain cytokine and chemokine mRNA expression in mice induced by intranasal instillation with ultrafine carbon black. Toxicol Lett 163:153–160

Wu HC, Yang CY, Hung DZ, Su CC, Chen KL, Yen CC, Ho TJ, Su YC, Huang CF, Chen CH, Tasi LM, Chen YW (2011a) Nickel (II) induced JNK activation regulated mitochondria dependent apoptosis pathway leading to cultured rat pancreatic β-cell death. Toxicology 289:103–111

Wu J, Wang C, Sun J, Xue Y (2011b) Neurotoxicity of silica nanoparticles: brain localization and dopaminergic neurons damage pathways. ACS Nano 5:4476–4489

Yadav RS, Sankhwar ML, Shukla Rk, Chandra R, Pant AB, Islam F, Khanna VK (2009) Attenuation of arsenic neurotoxicity by curcumin in rats. Toxicol Appl Pharmacol 240:367–376

Yoshida H (2007) ER stress and diseases. FEBS J 274:630–658

Zhang R, Piao JM, Kim KC, Kim AD, Choi JY, Choi J, Hyun JW (2012) Endoplasmic reticulum stress signaling is involved in silver nanoparticles-induced apoptosis. Int J Biochem Cell Biol 44:224–232